International Journal of Mineral Processing, 31 (1991) 163–193
Elsevier Science Publishers B.V., Amsterdam

The effect of liner design on the motion of the outer grinding elements in a rotary mill

M.S. Powell
MINTEK, Council for Mineral Technology, Private Bag X3015, Randburg 2125, South Africa

(Received February 28, 1990; accepted after revision, October 30, 1990)

ABSTRACT

Powell, M.S. 1991. The effect of liner design on the motion of the outer grinding elements in a rotary mill. *Int. J. Miner. Process.*, 31: 163–193.

A theoretical analysis was made of the motion of an isolated rod or ball, and the way in which it is influenced by a lifter bar of any face angle and of any height. The charge motion of rods in a glass-ended mill was filmed with a high-speed camera. The mill was fitted with a variety of lifter bars with different face angles and heights, and was run at a wide range of speeds. The trajectories of the rods on film were then tracked. The coefficients of friction between the rods and the lifter bar materials were measured under the vibrating conditions that are found in the mill.

It was found that there was a good correlation between the theoretical predictions and experimental results over a wide range of conditions. The impact point at which the grinding element strikes the shell of the mill was considered to be of primary importance in the analysis. It was found that as the height of the lifter bar increases from zero to slightly greater than one charge radius, the height has a strong influence on charge trajectories. Thereafter, the lift increases until a critical lifter-bar height is reached. At heights beyond this, the grinding element is projected off the lifter bar prior to reaching the tip, with the height of the impact point increasing slightly and then decreasing to a constant height. The change in the height of the impact point is very small, however, so, in practical terms, an increase in lifter-bar height — once it is higher than the radius of the grinding element — has only a slight effect upon the charge trajectories.

An increase in the angle of the lifter bars was found to have a strong influence upon the height of the charge trajectories. A linear relationship was discovered between the speed of the mill and the angle of impact, and changes in the mill speed strongly influence the charge trajectories.

Some surprising effects of lifter-bar geometry upon the charge trajectories have been discovered, and are of practical importance. The theoretical model is an improvement on all previous models, and agrees well with experimental results over a wide range of conditions.

INTRODUCTION

Rotary mills are used extensively in the size reduction of the coarse rocks of ores that are mined to a product fine enough to facilitate the extraction of the valuable minerals. The South African gold mines alone grind about 110 million tons of ore annually, at a power cost of about 140 million Rand and a liner material cost of about 40 million Rand (Powell, 1987).

0301-7516/91/$03.50

NOMENCLATURE

General variables

a	ball radius.
α	angular acceleration of ball.
δ	$\sin\alpha(R-h)-a \equiv a$ constant.
f	frictional force between face of lifter bar and ball.
F	resultant force on the ball.
g	gravitational acceleration ($9.8\ \mathrm{m\ s^{-2}}$).
h	radial height of lifter bar.
I	moment of inertia.
m	mass of ball.
N	normal force exerted by lifter bar on ball.
R	internal radius of mill.
r	distance from centre of mill to centre of ball.
$\vec{r}$	vector directed from centre of mill to centre of ball.
r_0	$R-a$.
s	$r\cdot\cos\beta$.
$\vec{s}$	vector parallel to face of lifter bar, directed from tip to base.
$\dot{s}$	linear velocity of ball along face of lifter bar.
$\ddot{s}$	linear acceleration of ball along face of lifter bar.
t	time.
τ	sliding time.
Γ	torque.
μ_s	static coefficient of friction between the ball and the lifter bar.
μ_k	kinetic coefficient of friction between the ball and the lifter bar.
v	net velocity of the ball, in cartesian coordinate system
Ω	angular velocity of the mill.
x	horizontal cartesian coordinate of the centre of the ball.
y	vertical cartesian coordinate of the centre of the ball.
$\perp$	perpendicular.
$\parallel$	parallel.

Angles

α	between lifter bar face and a radial line that passes through the tip of the lifter bar.
β	between radius vector to ball, and face of the lifter bar.
γ	subtended by $\vec{s}$ and x axis.
ϕ	subtended by $\vec{r}$ and x axis.
ρ	between the face of the lifter bar and its base.
σ	to horizontal of the velocity vector of the ball.
θ	subtended at centre, between the tip of the lifter bar and x axis.
λ	subtended at contact point of ball on lifter bar, between centre of ball and base of lifter bar.
κ	friction angle, equivalent to $\arctan\mu_s$.

Subscripts

0	point of equilibrium.
L	tip of lifter bar.
cm	about centre of mass of ball.
m	maximum.
I	point of transition from rolling to sliding.
ρ	point of contact between ball and the face of the lifter bar.
x	in direction of x.
y	in direction of y.
E	point at which ball strikes the shell of the mill.
$\parallel$	parallel to.
r	radial component.
$\perp$	perpendicular to.

Because the charge motion in mills has a determining influence on the grinding action, it has been studied, both theoretically and experimentally, since the beginning of the century. The influence of lifter bars upon charge motion has been considered only in the past few decades, and mostly to a very limited extent, as was revealed in an extensive survey of existing literature (Powell, 1988). This has left the field wide open to further research.

In this paper, a mathematical model of the motion of an isolated grinding element in a rotary mill is developed, which is then compared with experimental observations of the motion in a model mill. The specific aspect that is examined is the influence of the liner profile upon the motion of the outer layer of charge.

Studies by other investigators

In 1983 McIvor published a paper that examined the effect of liner configuration upon charge motion (McIvor, 1983). In this work, it was noted that the outer layer of the charge consumes a significant portion of the total input of power to the mill, and is also responsible for transfer of energy to the bulk of the charge. It was also concluded that the outer layer of charge has a significant effect on the motion of the bulk of the charge.

A theoretical analysis was made of the motion of a particle resting on a flat bar that projects out at an angle to the shell of the mill. It was assumed that at the moment that the particle reaches a state of equilibrium, i.e., the gravitational, centrifugal and frictional forces balance out, it is projected into free flight. It was concluded from these computations that the trajectories of the particles are highly sensitive to the leading face angle of the lifter bar. Although it was not revealed in the calculations, it was observed that the height of the lifter bar affects the trajectories.

In 1985, Vermeulen published a paper which analysed the lifting action of lifter bars (Vermeulen, 1985). In this work, some previously unappreciated factors were brought to light. Vermeulen recognised that the width of the bar affects the angle of its leading face and, most importantly, that the particle is not projected into flight from the base of the bar. From the equations of force, it is apparent that the particle remains in contact with the lifter bar, and rolls or slides down the face until it reaches the tip of the bar, at which point it is projected into flight. This revealed the way in which the height of the lifter bar affects the degree of lift of the particles.

Vermeulen's work gave a sound foundation upon which a theoretical model of charge motion could be developed, and the analysis given here is based upon the techniques that he used.

THEORY

A theoretical study follows of the effect that lifter bars of varying face angle and height have upon the outer layer of charge within a rotary mill. The simplest case of an isolated ball keyed-in to the motion of the mill is considered.

A ball resting on a lifter bar, and against the shell of a rotating mill, reaches a point of equilibrium where the sum of the forces acting on it is zero. Here, the net forces on the ball, parallel to ($\parallel$) and radially perpendicular to ($\perp$) the motion of the ball, are zero. The ball will then start to roll or slip down the face of the lifter bar (Vermeulen, 1985).

Point of equilibrium

With reference to Figs. 1 and 2, the forces acting on the ball are as follows:

(a) gravitational force, acting vertically downwards (mg),

(b) centrifugal force directed radially outwards towards the mill shell ($m\Omega^2 r$),

(c) normal force of the lifter bar (N), and

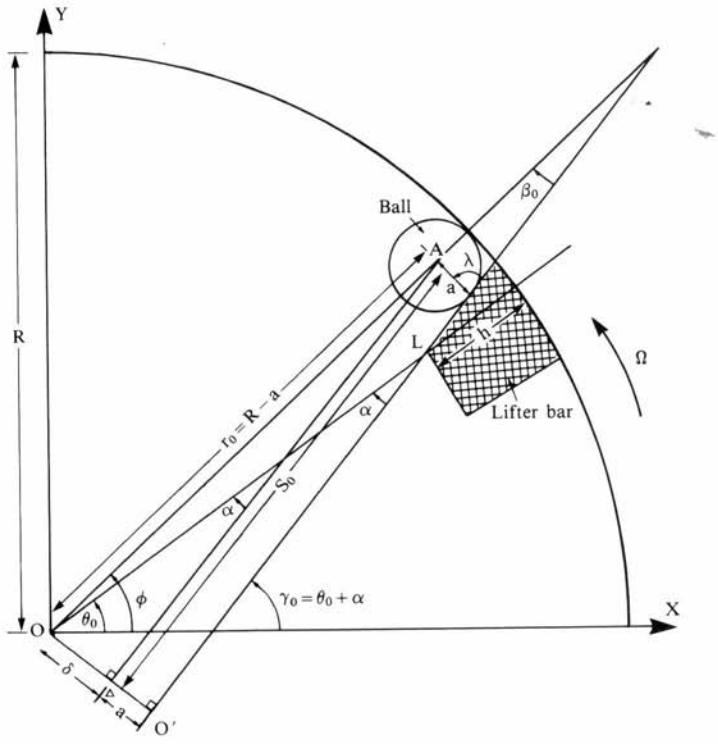

Fig. 1. Ball on a lifter bar in a rotary mill.

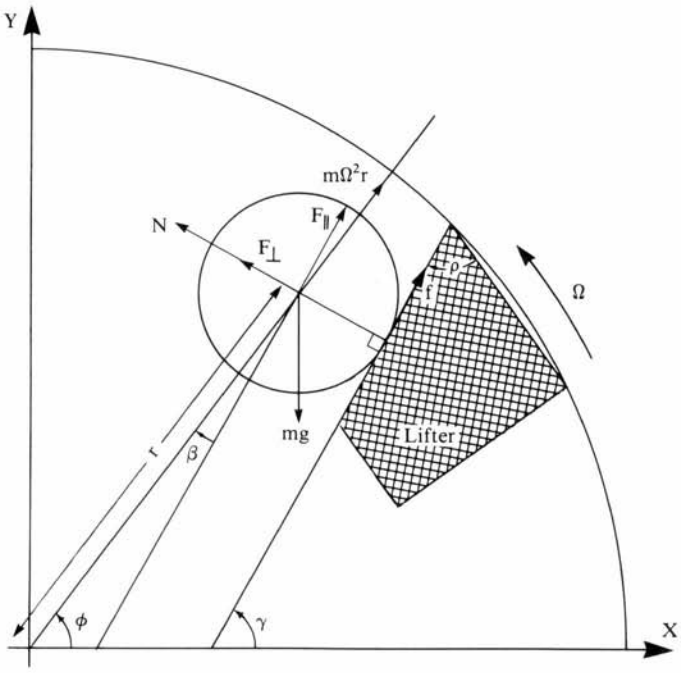

Fig. 2. Forces on a ball in contact with a lifter bar.

(d) frictional force between the ball and lifter bar, which is parallel to the face, and directed towards the mill shell (f).

For this analysis, the forces are resolved into components that are parallel and perpendicular to the leading face of the lifter bar, and in the plane of rotation of the mill.

All symbols that are used, are listed in Nomenclature and are also shown in Figs. 1 and 2. At the point of equilibrium we have forces that are ∥ to the face of the lifter bar:

$$m\Omega^2 r_0 \cdot \cos\beta_0 + \mu_s N - mg \cdot \sin\gamma_0 = 0 \tag{1}$$

and forces that are ⊥ to the face of the lifter bar:

$$N - mg \cdot \cos\gamma_0 - m\Omega^2 r_0 \cdot \sin\beta_0 = 0 \tag{2}$$

Substituting for N into eq. 1, and dividing by m, gives:

$$\sin\gamma_0 - \mu_s \cdot \cos\gamma_0 = \frac{\Omega^2}{g} r_0 (\cos\beta_0 + \mu_s \cdot \sin\beta_0) \tag{3}$$

Substituting $\tan\kappa$ for μ_s, where $\kappa \equiv$ friction angle, and multiplying by $\cos\kappa$ yields:

$$\sin\gamma_0 \cdot \cos\kappa - \cos\gamma_0 \cdot \sin\kappa = \frac{\Omega^2}{g} r_0 (\cos\beta_0 \cdot \cos\kappa + \sin\beta_0 \cdot \sin\kappa)$$

$$\sin(\gamma_0 - \kappa) = \frac{\Omega^2}{g} r_0 \cdot \cos(\beta_0 - \kappa)$$

$$\gamma_0 = \kappa + \arcsin\left(\frac{\Omega^2}{g} r_0 \cdot \cos(\beta_0 - \kappa)\right) \tag{4}$$

For $\vec{s}$, which is the unit vector parallel to the face of the lifter bar and which is directed outwards, we can see from Fig. 1 that, at the point of equilibrium:

$$s_0 = r_0 \cdot \cos\beta_0 \tag{5}$$

$$\beta_0 = \arcsin\left(\frac{\delta}{r_0}\right) \tag{6}$$

where $\delta = (R-h) \cdot \sin\alpha - a \equiv$ constant.

By use of eqs. 4, 5 and 6 the location of the ball at the point of equilibrium can be determined fully.

For a lifter bar that is lower in height than the radius of a ball, the angle λ is greater than 90°. This introduces additional terms into eqs. 1 and 2, which involves both sin and cos functions of N. The solution for the point of equilibrium is given by:

$$\gamma_0 = \kappa - \lambda + \arccos\left(-\frac{\Omega^2}{g} r_0 \cdot \sin(\lambda + \beta_0 - \kappa)\right) \tag{7}$$

The ball is already at the tip of the bar, and is therefore projected directly into flight from the point of equilibrium.

When the ball is at the tip of the lifter bar, the distance s_L and the angle β_L are given by the condition that $s_L = \overline{LO'}$ (Fig. 1). Therefore, from $\Delta\, OLO'$:

$$s_L = (R-h) \cdot \cos\alpha \tag{8}$$

$$\beta_L = \arctan\left(\frac{\delta}{s_L}\right) \tag{9}$$

Between the point of equilibrium and the tip of the lifter bar the ball rolls and slides down the face of the bar. It is not projected into free flight from the point of equilibrium because while N is finite, the ball must interact with the lifter bar. It can happen that the face of the lifter bar is almost vertical, i.e. $\gamma \simeq 90°$, while the ball is still in contact with the bar. In this case, the ball will fall away from the lifter bar once the normal force N is zero, i.e.:

$$m\Omega^2 r \cdot \sin\beta + mg \cdot \cos\gamma = 0$$

$$g \cdot \cos\gamma + \Omega^2 \delta = 0 \tag{10}$$

All calculations must be checked continuously for this condition, as the following derivations apply where N is positive and the ball remains in contact with the face of the lifter bar until it reaches the tip of the bar.

If the static coefficient of friction is greater than zero, the ball will initially undergo pure rolling due to the torque applied by f (Fig. 2), where:

$$f \leq \mu_s N$$

Ball rolling down the face of the lifter bar

If the forces that act on sphere as it rolls down a slope that is subjected to a constant angular velocity are considered, the following equations can be derived, using Fig. 3:

$$\text{normal to incline}: N - mg \cdot \cos\gamma - m\Omega^2\delta = 0 \tag{11}$$

$$\text{in plane of incline}: m\Omega^2 s - mg \cdot \sin\gamma + f = m\ddot{s} \tag{12}$$

$$\text{torque about centre of mass (cm)}: \Gamma_{cm} = I_{cm}\alpha \tag{13}$$

where $\gamma = \gamma_0 + \Omega t$.

The only force that acts at a distance from the centre of mass is f, so:

$$f \cdot a = I_{cm}\alpha$$

For a sphere:

$$I_{cm} = \frac{2}{5} ma^2$$

This moment of inertia about the centre of mass is the only factor that differentiates between the motion of a ball and a rod when rolling down a plane. For a rod, $I_{cm} = \frac{1}{2} ma^2$, which is the only factor that needs to be changed in order for the calculations to be applied to rods.

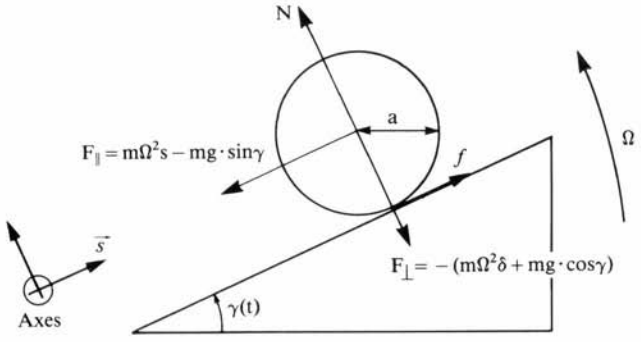

Fig. 3. Forces on a sphere rolling down a slope of changing incline, $\gamma(t)$.

While the ball doesn't slip, the angular acceleration is directly related to the linear acceleration by:

$$\alpha = -\frac{\ddot{s}}{a} \tag{14}$$

where $\ddot{s}$ is negative for a positive α, as a result of the orientation of the axes. Hence:

$$f = -\frac{2m\ddot{s}}{5} \tag{15}$$

The substitution of this into eq. 12 yields:

$$\ddot{s} - \frac{5}{7}\Omega^2 s = -\frac{5}{7} g \cdot \sin\gamma \tag{16}$$

The solution of this linear, non-homogenous second-order differential equation, which is consistent with the boundary conditions of $s(0) = s_0$, which is known, and $\dot{s}_{t=0} = 0$ (as the ball has not yet started rolling) is:

$$s(t) = \left(s_0 - \frac{5g}{12\Omega^2} \cdot \sin\gamma_0\right) \cdot \cosh \sqrt{\frac{5}{7}} \cdot \Omega t - \frac{\sqrt{35}\, g}{12\Omega^2} \cdot \cos\gamma_0 \cdot \sinh \sqrt{\frac{5}{7}} \cdot \Omega t + \frac{5g}{12\Omega^2} \cdot \sin\gamma \tag{17}$$

$$\dot{s} = \sqrt{\frac{5}{7}}\, \Omega \left(s_0 - \frac{5g}{12\Omega^2} \cdot \sin\gamma_0\right) \cdot \sinh \sqrt{\frac{5}{7}} \cdot \Omega t - \frac{5g}{12\Omega} \cdot \left(\cos\gamma_0 \cdot \cosh \sqrt{\frac{5}{7}} \cdot \Omega t - \cos\gamma\right) \tag{18}$$

These equations describe the position and velocity of the ball for pure rolling down the face of a lifter bar.

Maximum angle for pure rolling

There is a limit on the force (f) given by $\mu_s N$, so, for a given static coefficient of friction (μ_s) and mill parameters, there is a maximum angle (γ_m) up to which pure rolling will occur. Beyond this angle, the linear acceleration is too high for eq. 14 to hold, and the surface of the sphere must begin to slip across the face of the lifter bar. The theoretical maximum angle for pure rolling can be calculated from the equations that express the forces on the rolling sphere, and that give its acceleration. The substitution of eq. 16 into eq. 12 yields:

$$f=\frac{2m}{7}(g\cdot\sin\gamma-\Omega^2 s) \tag{19}$$

$f\leq\mu_s N$, so from eqs. 11 and 19:

$$\sin\gamma_m-\frac{7}{2}\mu_s\cdot\cos\gamma_m\leq\frac{\Omega^2}{g}\left(\frac{7}{2}\delta\mu_s+s\right) \tag{20}$$

However, $s=s(t)$, so this can only be solved numerically. The solution of eq. 20 when $s=s_L$ yields $\gamma_m(\min)$, which is the minimum possible value of γ_m at the limit. Equation 17 can then also be numerically solved for $s=s_L$. However, if $\gamma_L>\gamma_m(\min)$, then there must be a transition from pure rolling to rolling and sliding.

Transition from pure rolling to combined rolling and sliding

The simultaneous solving of the eqs. 20 and 17 for γ_m and $s(t)$ yields the limit for pure rolling. The resulting equation:

$$\frac{7}{12}\sin\gamma_m-\frac{7}{2}\mu_s\cdot\cos\gamma_m\leq \tag{21}$$

$$\frac{7\Omega^2}{2g}\delta\mu_s+\left(\frac{s_0}{g}\Omega^2-\frac{5}{12}\sin\gamma_0\right)\cosh\sqrt{\frac{5}{7}}\cdot\Omega t_1-\frac{5\sqrt{3}}{12}\cdot\cos\gamma_0\cdot\sinh\sqrt{\frac{5}{7}}\cdot\Omega t_1$$

can be solved by increasing t until the inequality is satisfied for $t=t_1$, where t_1 is the time at which the transition from rolling to sliding takes place. By use of eqs. 17 and 18, the location and velocity of the ball can be calculated at this transition point.

Combined rolling and sliding

Once the ball begins to slide, its motion is retarded by the force arising from the kinetic coefficient of friction. A combination of rolling and sliding yields a linear motion that is equivalent to pure sliding under friction. As there is a torque about the centre of mass, there must still be an angular acceleration of the ball about its centre of mass, but under sliding conditions this is not dependent upon the linear motion. Some of the gravitational energy that would otherwise be lost due to friction, in the case of a flat-bottomed block, is instead converted to rotational motion of the ball about its centre. From eq. 13 it is derived that:

$$f\cdot a=\frac{2}{5}ma^2\cdot\alpha$$

Now:

$$f=\mu_k \cdot N=\mu_k(mg\cdot\cos\gamma+m\Omega^2\delta)$$

so:

$$\alpha=\frac{5\mu_k}{2a}(g\cdot\cos\gamma+\Omega^2\delta) \tag{22}$$

which yields the angular acceleration of the ball once it starts sliding.

Sliding

When pure sliding down the face of the lifter bar is considered, and (with reference to Fig. 2) the forces are resolved parallel and perpendicular to the face of the lifter bar, we have the following:
$\parallel$ to the face of the lifter bar:

$$m\Omega^2 r\cdot\cos\beta+\mu_k N-mg\cdot\sin\gamma=m\cdot\ddot{s} \tag{23}$$

$\perp$ to the face of the lifter bar:

$$N-mg\cdot\cos\gamma-m\Omega^2 r\cdot\sin\beta=0 \tag{24}$$

The linear acceleration is found by the substitution for N into eq. 23 and the expression of this in terms of s and δ:

$$\ddot{s}-\Omega^2 s=g(\mu_k\cdot\cos\gamma-\sin\gamma)+\Omega^2\mu_k\delta \tag{25}$$

From the transition point, it is easiest to start with a new time, which can be designated by τ. The boundary conditions at $\tau=0$ are given as:

$s(0)=s_1$ and $\dot{s}_{\tau=0}=\dot{s}_1$

The solution of this differential equation that is consistent with these boundary conditions is:

$$\begin{aligned} s(\tau)=&\left[s_1+\mu_k\delta+\frac{g}{2\Omega^2}(\mu_k\cdot\cos\gamma_1-\sin\gamma_1)\right]\cosh\Omega\tau \\ &+\left[\frac{\dot{s}_1}{\Omega}-\frac{g}{2\Omega^2}(\mu_k\cdot\sin\gamma_1+\cos\gamma_1)\right]\sinh\Omega\tau \\ &-\frac{g}{2\Omega^2}[\mu_k\cdot\cos(\gamma_1+\Omega\tau)-\sin(\gamma_1+\Omega\tau)]-\mu_k\delta \end{aligned} \tag{26}$$

$$\dot{s}=\Omega\left[s_1+\mu_k\delta+\frac{g}{2\Omega^2}(\mu_k\cdot\cos\gamma_1-\sin\delta_1)\right]\sinh\Omega\tau$$
$$+\left[\dot{s}_1-\frac{g}{2\Omega}(\mu_k\cdot\sin\gamma_1+\cos\gamma_1)\right]\cosh\Omega\tau \qquad (27)$$
$$-\frac{g}{2\Omega}[-\mu_k\cdot\sin(\gamma_1+\Omega\tau)-\cos(\gamma_1+\Omega\tau)]$$

Equation 26 is solved numerically for $s(\tau)=s_L$, and yields τ, which in turn yields the velocity and position, γ, for the ball at the tip of the lifter bar. The τ that is used starts at zero at the transition point between rolling and sliding, so that the total time moving along the lifter bar is $t_L=t_1+\tau$.

Free-flight trajectory

At the tip of the lifter bar the ball is immediately projected into free flight, as there is no further significant interaction with the tip of the bar as a result of the radial velocity of the ball, and the curve of its surface. Figure 4 illustrates clearly the reason why the ball escapes (Vermeulen, pers. commun., 1989). As the ball is a rigid object, all its parts travel with the same velocity as the centre of the ball, which causes a difference in velocity between the point of the ball that is in contact with the tip of the lifter bar and the tip itself. It can be seen that even if the ball does not have a radial velocity, i.e., for a lifter bar with a height that is the same as or less than a ball radius, there is a velocity difference between the ball and the tip of the lifter, and this has a radial component which allows the ball to escape from the lifter bar without

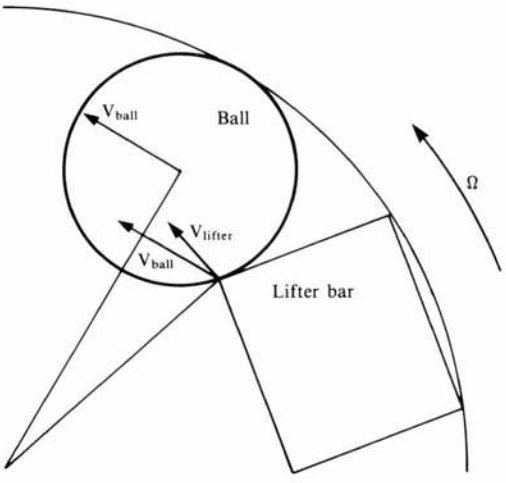

Fig. 4. Resolution of the velocities for a ball resting on the tip of a lifter bar.

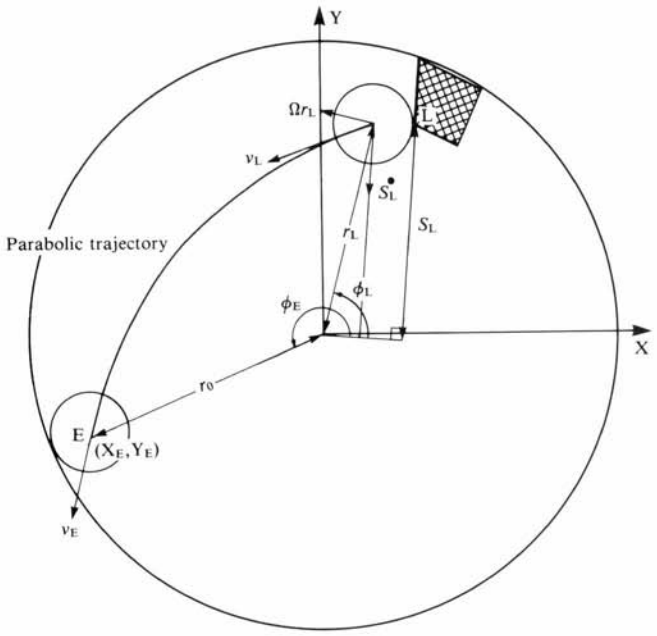

Fig. 5. Parabolic trajectory of the ball at its point of departure from the lifter bar.

interaction at the tip. If the lifter bar is worn or rounded at the tip, then the point at which the rounding begins is effectively the tip. The curvature of the surface of the lifter bar results in a decreasing face angle, and the lower the face angle of the lifter bar, the less the lift of the ball. Therefore, as soon as the ball, moving along the lifter bar, encounters a lower face angle, it must fall free of the bar. For a lifter bar that curves from the base, the ball must be projected into free flight from the point of equilibrium, and will not move along the bar at all.

The free-flight trajectory is illustrated in Fig. 5. At the tip of the lifter bar, the following is known: $\dot{s}_L$, s_L, θ_L, β_L, γ_L. The radial coordinates of the ball are:

$$(r_L; \phi_L) = \left(\frac{s_L}{\cos\beta_L}; \gamma_L - \beta_L \right) \tag{28}$$

So that the free-flight trajectory can be determined, it is convenient to change the frame of reference to Cartesian coordinates, with the origin at the centre of the mill:

$$(x_L, y_L) = (r_L \cdot \cos\phi_L, r_L \cdot \sin\phi_L) \tag{29}$$

$\dot{s}_L$ is the velocity of the ball along the face of the lifter bar, to which the velocity due to the rotation of the mill must be added. This velocity component is tangential, and equals Ωr_L:

$$(v_{xL}; v_{yL}) = (\dot{s}_L \cdot \cos\gamma_L - \Omega r_L \cdot \sin\phi_L; \dot{s}_L \cdot \sin\gamma_L + \Omega r_L \cdot \cos\phi_L) \tag{30}$$

The net velocity is:

$$v_L = \sqrt{v_{xL}^2 + v_{yL}^2} \tag{31}$$

the angle of projection is:

$$\sigma_L = \arctan\left(\frac{v_{yL}}{v_{xL}}\right) \tag{32}$$

to the horizontal.

Once in free flight the ball follows a parabolic path, which is given by:

$$x = x_L + v_{xL}t \tag{33}$$

$$y = y_L + v_{yL}t - \tfrac{1}{2}gt^2 \tag{34}$$

The point at which the ball strikes the shell of the mill, assuming that no interaction with the charge mass occurs en route, is satisfied by the condition:

$$x_E^2 + y_E^2 = r_0^2 \tag{35}$$

The velocity components are given by:

$$(v_{xE}; v_{yE}) = (v_{xL}; v_{yL} - gt) \tag{36}$$

so the velocity of impact with the mill shell is:

$$v_E = \sqrt{v_{yE}^2 + v_{xE}^2} \tag{37}$$

at an angle σ_E to the horizontal:

$$\sigma_E = \arctan\left(\frac{v_{yE}}{v_{xE}}\right) \tag{38}$$

The full path of the ball in flight, and its conditions of impact with the shell, have thus been derived.

This completes the theoretical analysis of the motion of an isolated ball in a rotary mill with flat-faced lifter bars of any face angle and of any height.

EXPERIMENTAL

Filming of the charge motion

A glass-ended drum, 387 mm in diameter and 300 mm in length, which was driven by an asynchronous electric motor connected to a variable speed gearbox, formed the experimental mill. The mill was fitted with 16 removable lifter bars, and five sets of rectangular section (90°) bars, 6.3, 12, 14.4, 20 and 25 mm in height were used. There were also four sets of lifter bars having face angles of 75, 60, 45 and 30 degrees. The mill was loaded with rods of 12

mm in diameter. The mill was run at seven different speeds; from 60 to 100% of the critical speed. Rods were used so that the end effects of the glass could be minimized, because the end plates provide an added lifting action to the grinding media, thus distorting the observed results when a ball charge is used. In addition, the balls migrate away from the end window, making it difficult to trace a particular one over an extended period.

It should be noted that the equations for a rod were used in the comparisons of the experimental and theoretical results.

A variable-speed 16-mm camera was used in the filming of the charge motion, and a speed of around 300 frames per second was used. A wooden information board was mounted in front of, and surrounding the mill. Horizontal and vertical lines were centred about the centre axis of the mill, which acted as a reference marker for the analysis of the films. It was ensured that the camera was aligned both centrally and perpendicularly relative to the face of the mill, so that the problems of parallax and distortion could be avoided. A constant-speed asynchronous motor, running at 200 r min^{-1}, had a pointer mounted on its shaft, and in front of a dial face, to form a high-speed clock that was visible on the films.

Analysis of the films

The primary aim of the film analysis was to plot the trajectories of individual rods in a way that would allow the predictions of the theoretical model to be compared with these trajectories, and so that a visual record of the charge motion could be formed. The film analysis was carried out by the projection of the film, frame by frame, onto a graphics tablet. The positions of the rods were then recorded directly from the tablet by use of a mouse, which was linked to a computer.

A circle, which filled the full area of the graphics tablet, was drawn as a template upon which the image of the mill could be projected and located. The horizontal and vertical lines that were located about the centre point were marked on the edge of the circle. This allowed the image to be accurately located by the similar lines on the information board. In general, the tip of a lifter bar, and the four rods in front of it, were followed. The speeds of the mill and the camera were checked for each run, by use of the clock mounted next to the mill.

Lifter-bar vibration

The mill vibrated extensively while it rotated, and it was realised that this would have a large effect on the coefficient of friction between the lifter bar and the rod resting on it. It was therefore decided to measure the principal frequency at which a lifter bar vibrated. An accelerometer was screwed di-

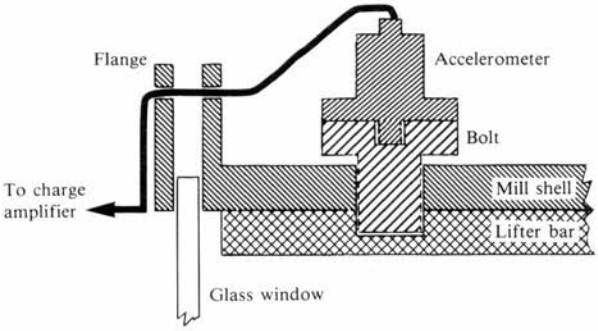

Fig. 6. Layout of the accelerometer.

rectly into a lifter bar, as is illustrated in Fig. 6. A cable was taken from this through a bolt hole in the flange, and was then connected to a charge amplifier which was linked to a storage oscilloscope.

The mill was run with a standard 40% charge, and a signal was triggered on the oscilloscope in the storage mode. Data was accumulated over a number of revolutions of the mill. The principal frequency of vibration was sought across the frequency spectrum, and the period was then measured directly off the screen, and checked for reproducibility.

Measurement of the coefficients of friction

It was decided that a simple experiment should be carried out in which a sample slides down an inclined plane. A steel sheet (1 m in length) was machined in the same manner as the lifter bars, and was mounted onto a variable-angle rack. A rod was cut into four pieces which were then welded together to form a square that could act as the sliding sample. The sliding surfaces thus formed the same contacting pair of materials as is present in the rod/lifter-bar interface. The apparatus was placed onto thick foam sheets, and a vibrator was screwed onto the end of the rack. A standard video camera was used to film the motion of the sliding sample, and a video recorder with a special frame-by-frame advancing facility was used to analyse the film.

So that the static coefficient of friction could be measured, the sliding piece was placed on the surface, and the surface was gradually lifted until the angle at which the sample began to slip was reached. This was repeated a few times so that the angle could be accurately checked. The sliding piece was placed with the rod sections perpendicular to the direction of motion, as occurs under real conditions in the mill.

The kinetic coefficient of friction was determined from the sliding time of the sample — from the moment of release at the top to a fixed point near the base — and the slope was tilted to an angle that allowed the sample to slide

freely. Static and kinetic coefficients of friction were measured at the following frequencies: stationary, 10, 100, 300, 600 and 1000 Hz. Two amplitudes of vibration were tested for each frequency, and it was found that 1000 Hz was the limit of response of this heavy rig to the vibrator.

RESULTS

Films of charge motion

The different sizes and shapes of the lifter bars yielded clearly discernible differences in the motion of the charge, both in the outer layers and in the bulk of the charge. Figure 7 gives a plot of the paths of two different rods in

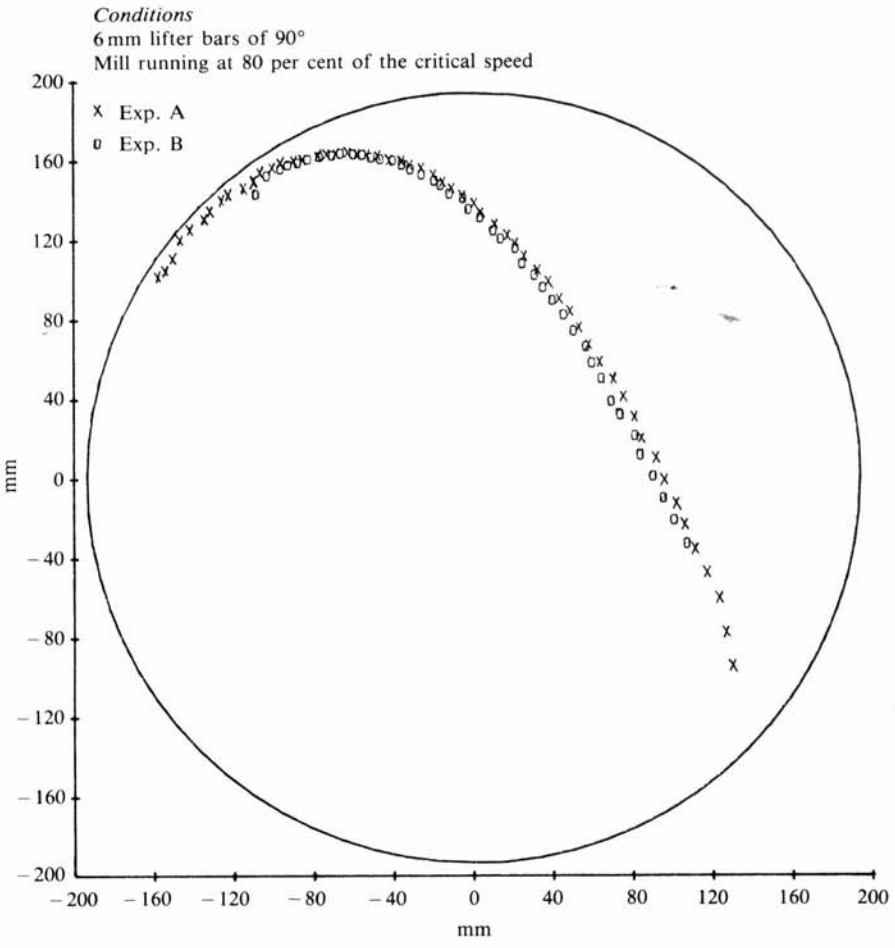

Fig. 7. Comparative plots of rod trajectories during a single run.

the same run, which illustrates the expected reproducibility of the rod trajectories.

With the runs in which perpendicular lifter bars were used, it was noticed that the rods were projected separately off the lifter bar. In particular, the rod that was against the bar was free of the others before it started to move down the lifter bar. However, with sloping-faced lifter bars, the rods slid off in groups; the one that was against the bar was pushed off first. This clustered projection made it difficult to locate isolated rods that were being projected off the sloping-faced lifter bars. Figure 8 illustrates some of the plots that show

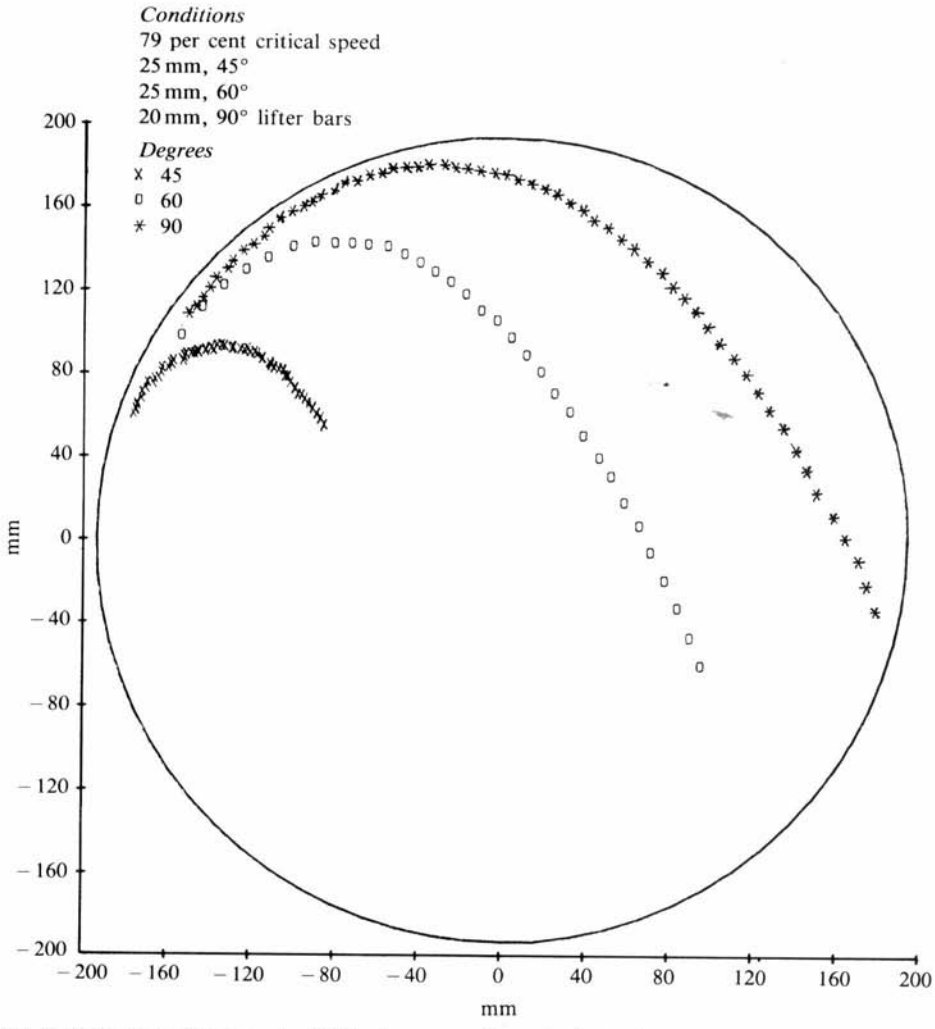

Fig. 8. Influence of face angle of lifter bar upon charge trajectories.

the large influence that the lifter-bar face angle has upon the trajectories of the rods.

Lifter-bar vibration

When the mill was run continuously for about a minute, a major 70-μs period peak was obtained that had an amplitude of about 10 times that of the subsidiary peaks. This indicates that the lifter bar has a principal frequency of vibration of 14.3 kHz.

The coefficients of friction

A list of the variations in the apparent static coefficient of friction under a range of vibrating conditions is given in Table 1. It was somewhat difficult to judge the exact angle at which the sample began to slide. However, the observed variation was not great, and was estimated to be within 1°, yielding an uncertainty of ± 0.015 in the coefficient of friction. Although the results only extend up to 1 kHz, it is clear that the apparent static coefficient of friction is tending to zero, and will be approximately zero when the sample rests upon the surface of a lifter bar that is vibrating with a frequency of 14 kHz.

The kinetic coefficient of friction is calculated according to the following equation:

$$\mu_k = \frac{\sin\gamma - 2d/gt^2}{\cos\gamma} \tag{39}$$

where d is the length of the sliding surface, γ is the angle and t the sliding time.

The results of the measurements of the apparent kinetic coefficient of fric-

TABLE 1

Apparent static coefficient of friction

Frequency (Hz)	Relative amplitude*[1]	Angle, γ (°)	μ_s
0		13	0,23
10	1	13	0,23
100	1	13,5	0,24
	2	7	0,12
300	1	10	0,18
	2	4	0,07
600	1	7	0,12
	2	5,5	0,10
1000	2	5	0,09
	4	<3	0,05

*[1]The relative amplitude is the amplitude setting on the vibrator.

TABLE 2

Apparent kinetic coefficient of friction

Frequency (Hz)	Amplitude	Number of frames							Time (s)	μ_k
		1	2	3	4	5	6	Avg		
0	0	62	58	64	66	68	64	64	1,28	0,22
10	1	59	58	59	60	58		59	1,18	0,20
100	1	59	59	61	58	61	56	59	1,18	0,20
	2	57	57	59	59			58	1,16	0,20
300	1	58	55	58	56	59		57	1,14	0,19
	2	57	57	56	59	56		57	1,14	0,19
600	1	59	56	54	57	58	56	57	1,14	0,19
	2	56	58	56	57	56	57	57	1,14	0,19
1000	2	55	57	59	59	53	54	56	1,12	0,19
	4	58	56	56	54	54		56	1,12	0,19

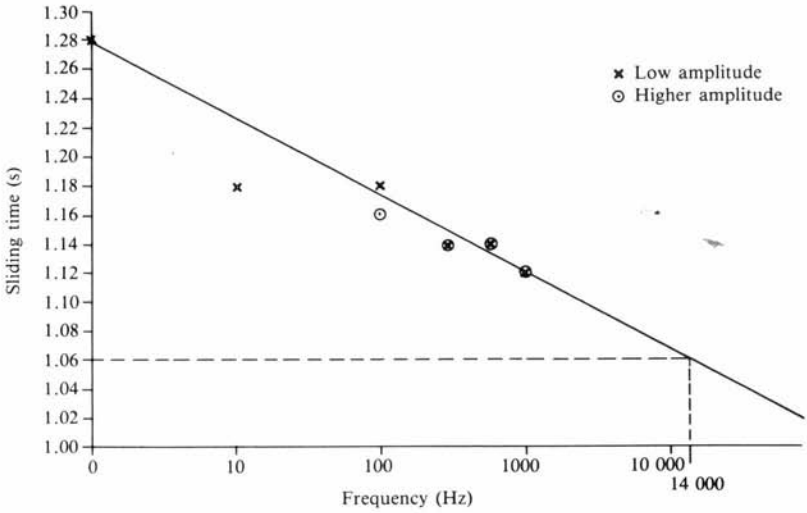

Fig. 9. Measurements of apparent kinetic coefficient of friction; sliding time for different frequencies of vibration.

tion are given in Table 2. If, in increasing the frequency of vibration to 14 kHz, the sliding time, (t) decreases by 0.06 s (which, from an inspection of Fig. 9, appears likely), then the error in t is 5.4%. As μ_k is a function of t^2, the error in μ_k is about 11%. Therefore, it is estimated that μ_k has a high probability of being in the range 0.19 to 0.17. It is possible that the sliding time could decrease even further if the simple extrapolation of the curve that is fitted to the times is incorrect, in which case μ_k could be somewhat lower.

As μ_s and μ_k are central to the theory, it is important that the influence of the uncertainty in these quantities on the theoretically predicted rod trajec-

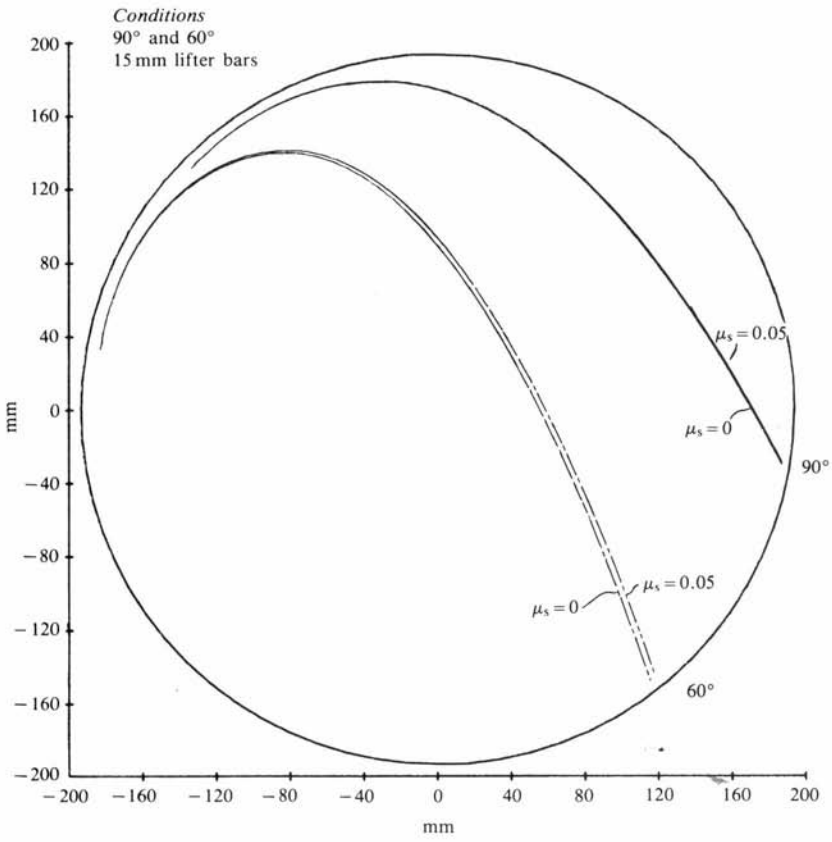

Fig. 10. Influence of varying μ_s upon the rod trajectory.

tories be illustrated. Figure 10 shows the influence that the variation of the apparent static coefficient of friction from 0 to 0.05 has on the trajectories. The change in the trajectory of rods with lifter bars of 90° is negligible. When lifter bars of 60° are used in the mill, the change in trajectory is slightly greater, but within the experimental uncertainties. The experimental evidence which indicates that the apparent static coefficient of friction is approximately zero, is sufficiently strong, and the variation in trajectories with μ_s is sufficiently small, for any error arising out of the uncertainty in the apparent static coefficient of friction to be considered negligible in this analysis.

Figure 11 illustrates the effect that the reduction of the kinetic coefficient of friction has upon the rod trajectories that result. When lifter bars of 90° are used, the influence upon the trajectories in reducing μ_k from 0.19 to 0.17 is almost indiscernible. Even a reduction to 0.10 has only a small effect. However, when lifter bars of 60° are used, the change in rod trajectories is significant, even with a 0.02 reduction in μ_k. The reduction of μ_k to 0.10 has a large

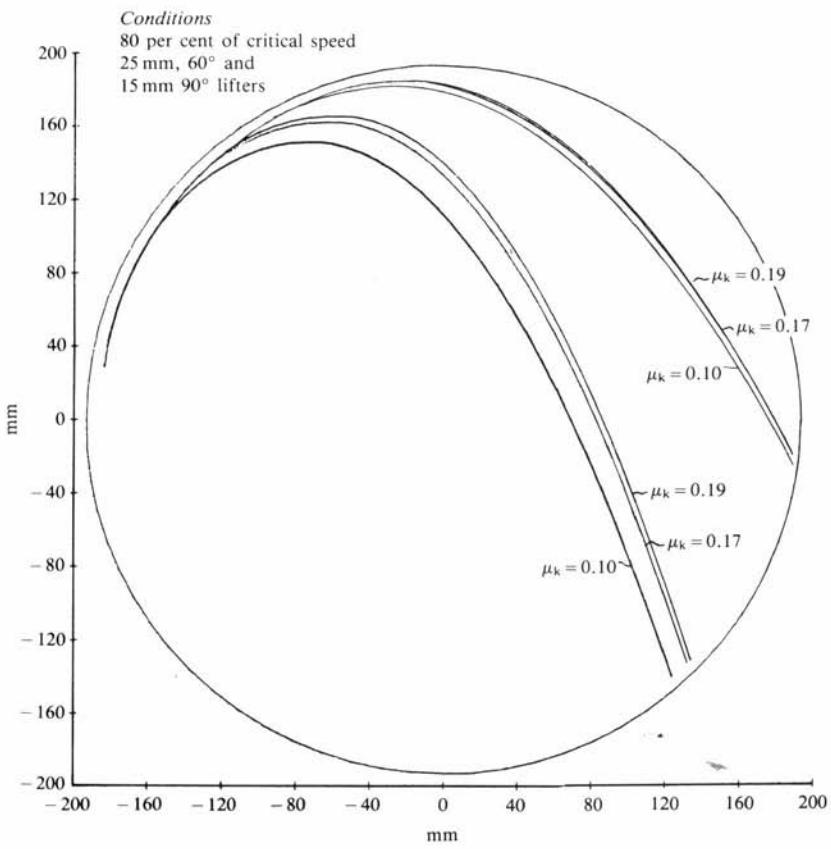

Fig. 11. Influence of reducing μ_k upon the rod trajectories.

influence upon the predicted rod trajectories. Uncertainties in the coefficients of friction will have little effect upon the predicted trajectories for perpendicular lifter bars, but could introduce a significant error in the predicted trajectories for sloping-faced lifter bars.

DISCUSSION

Figure 12 illustrates particular points in the trajectories of the rods, as these shall be repeatedly referred to during the course of this discussion.

Comparison of the theory with experimental results

A computer programme was written which enabled the rapid calculation of rod trajectories under varying conditions. The equations that were derived for ball motion were converted where necessary, so that the different moment

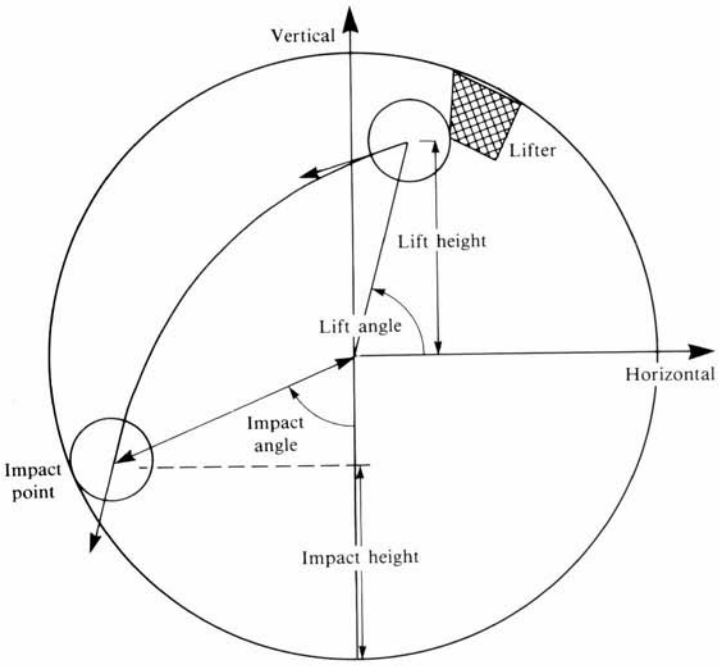

Fig. 12. The lift and impact points of a rod.

of inertia of the rods could be allowed for. The following factors varied in the experiments: face angle of the lifter bar, height of the lifter bar and speed of the mill. There are no adjustable variables, and all variables are either experimentally determined, or fixed by given experimental conditions. The theory can therefore not be adjusted to fit the results. It was considered that the best method of comparison was to plot predicted and experimentally determined rod trajectories together, which was carried out for a wide range of conditions, by use of the experimentally determined coefficients of friction of $\mu_s = 0$, and $\mu_k = 0.19$.

Figure 13 gives trajectories for a range of mill speeds and, on the whole, the correlation is excellent. The plot at a critical speed of 60.6% can be considered to be within the experimental uncertainties. Figure 14 gives a comparative plot of the range of trajectories that result from an increase in the height of the lifter bars. The theory predicts the same surprising result as the experimental work, namely that the higher lifter bars do not project the rods as high as the lower lifter bars. It was found that the 6-mm lifter bars had not been properly machined, which resulted in a rounded leading edge and an incorrect height. The exact height is crucial for lifter bars which are close to the radius of a rod in height, so small variations yield significant errors, which result in

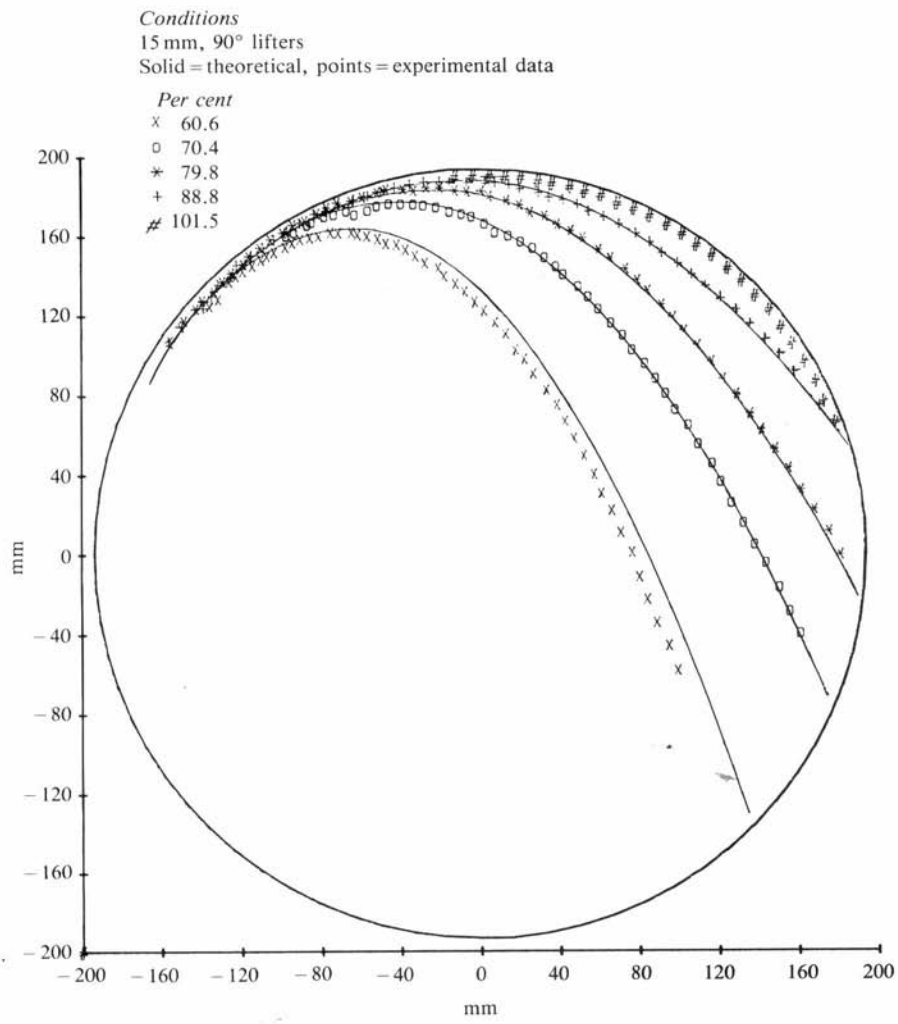

Fig. 13. Comparison of theoretical and experimental trajectories over a wide range of speeds.

a significant discrepancy between the derived and measured trajectories for the 6-mm lifter bars.

Analysis of the theory

Now that it has been established that the theory provides a good prediction of the influence of lifter bars and mill speed upon the rod trajectories, the theory can be analysed to provide a deeper insight into the effects that were observed.

A plot of the mill speed versus the impact angle yields a surprising result

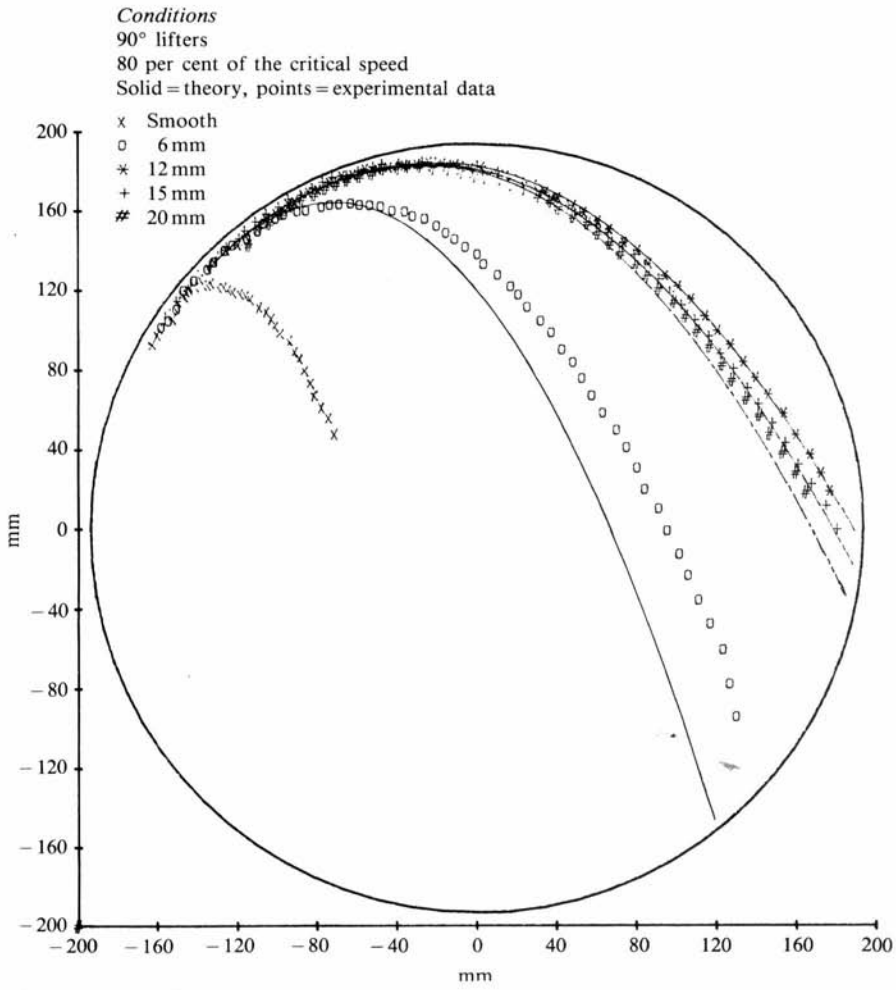

Fig. 14. Comparison of theoretical and experimental trajectories for a range of lifter-bar heights.

which, as given in Fig. 15, shows that there are two linear regions. A linear regression carried out on the principle region, from 60 to 84% of the critical speed, yields a coefficient of correlation of 0.9999, and is therefore linear. There is a distinct inflection of the line at a value of 85% of the critical speed, which is followed by a second minor linear region. This inflection occurs because, under these particular conditions, at above 85% of the critical speed, the rod is projected off the lifter bar prior to reaching the tip of the bar. As a result, a new set of controlling conditions apply. The second linear region has a steeper gradient than the major region. This occurs because the factors, which are discussed in the following section, that lower the trajectory of the rod no

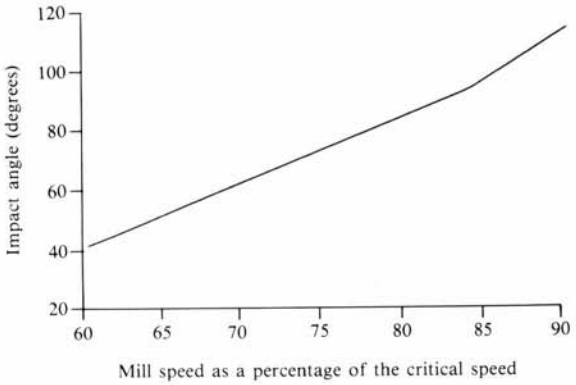

Fig. 15. The relationship between the speed of the mill and the angle of impact.

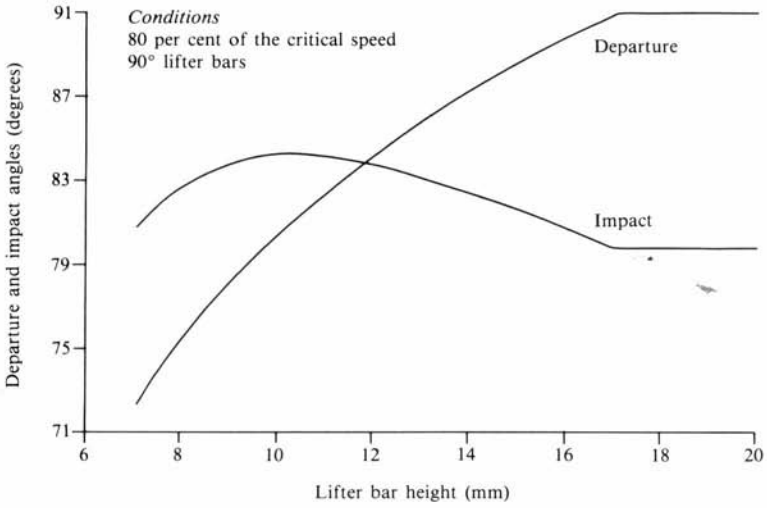

Fig. 16. The relationship between the height of the lifter bar and the angles of departure and impact.

longer apply, as the rod is not rolling any further along the lifter bar with the increasing mill speed, as is the case at below 85% of the critical speed.

Once the height of a lifter bar is greater than the radius of the rod, it exerts only a small effect upon the trajectory of the rods, as shown in Fig. 16. There is a peak in the projected angle of impact for a lifter bar height that is about equal to a rod diameter, after which the angle of impact drops off slightly. The underlying cause of this drop-off in the height of the trajectory is the radial acceleration of the rod. As the rod slides along the face of the lifter bar, the radial velocity increases relative to the tangential component of the velocity. In addition, the face of the lifter bar becomes progressively more vertical as

it lifts the rod higher, and the rod is projected off at a more horizontal angle. Thus, although the net velocity at the moment of projection off the lifter bar increases with an increase in the height of the lifter bar, the initial velocity vector of the free-flight trajectory is progressively directed further downwards. The direction factor gradually dominates the velocity factor, and leads to a shallower trajectory.

For most lifter-bar heights the angle of departure increases steadily with an increase in the height of the lifter bar, which is to be expected. However, above a critical lifter-bar height, which is dependent upon the speed of the mill and the face angle of the lifter bar, the rods follow identical trajectories which are independent of the height of the lifter bar. This occurs because the rod is projected off the face of the lifter bar prior to reaching the tip, as is shown in Fig. 16, by the constant angle of departure above a lifter bar height of 17 mm. This condition arises when the face of the lifter bar is close to perpendicular, and so the gravitational acceleration acting on the rod is directed away from the face of the lifter bar, thus causing the rod to accelerate away from the face. The escape of the rod from the face of the lifter bar is facilitated by the fact that, in moving towards the tip of the lifter bar, the tangential velocity of the face decreases as a result of its decreasing radius of rotation. As the tangential component of the rod's velocity increases due to the gravitational acceleration, the rod moves free of the lifter-bar face. The horizontal region on the impact-angle curve corresponds with this region of constant trajectories. The influence of the height of the lifter bar on the angle of impact is dependent upon the speed of the mill. At 60% of the critical speed, the angle of impact gradually increases and then levels out, without passing through a maximum. This is corroborated by the experimental results.

Figure 17 illustrates the large effect that the changing of the face angle of

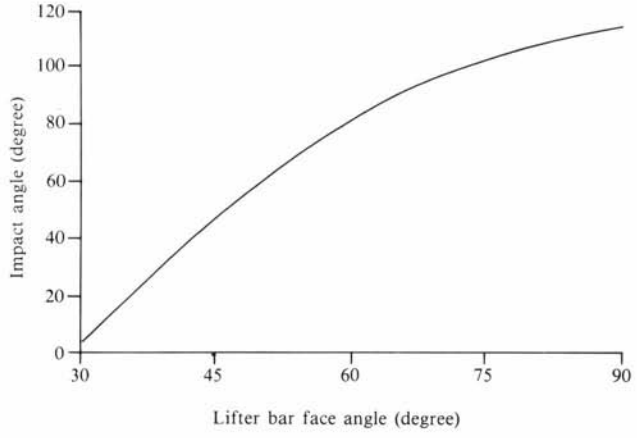

Fig. 17. The relationship between the face angle of the lifter bar and the angle of impact.

the lifter bar has upon the outermost rod trajectories. In this case of a high-speed mill, which runs at 90% of the critical speed, a perpendicular lifter bar projects the outer layer of charge high up onto the opposing face of the mill. The angle of the lifter bars can be tuned to project this outer layer onto the toe of the charge. In this instance, a lifter bar of 55° would be ideal. By use of this technique, lifter bars can be used to key in the bulk of the charge, without the projection of the outer layers onto the shell of the mill.

SCOPE AND VALIDITY OF THE WORK

A theoretical model, which is based on the fundamental laws of motion, was developed to describe the motion of an isolated rod or ball in a rotary mill, as affected by the geometry of the mill lining. This model takes into account both the static and the kinetic coefficient of friction that act between the grinding element and the lifter bar, and allowance is made for the rolling and slipping of the element. The model examines flat-faced lifter bars of any face angle and of any height. Only the outermost layer of charge is considered. However, this is an important indicator of the charge motion since it yields the outermost limits of the bulk charge motion.

In general, the correlation between the theoretical model and the experimental results is good, and indicates that the model gives the correct predictions of charge motion. However, the predictions are limited by the uncertainty in the measurement of the kinetic coefficient of friction, which arises from limitations in the experimental apparatus. This limitation has been shown to cast some uncertainty upon the predicted lifting action of the angled lifter bars. It appears, from a rough comparison with experimental data (the data not being suitable for a proper comparison), that the theory predicts higher trajectories than those found for angled lifter bars, which indicates that the actual value of the kinetic coefficient of friction is lower than the value of 0.19 that was used.

The theoretically predicted trajectories give good predictions of the outer charge motion, and all the predicted trends are correct. However, the limitations arising from the incertainty in the measurement of the kinetic coefficient of friction should be borne in mind.

Previous work examined the effect that lifter bars have upon the charge motion only to the point up to which the charge is lifted. However, both the full trajectory, and especially the impact point of the charge, are of great importance. In milling, it is desirable to key-in the charge to the rotary motion of the mill, but in so doing the charge should not be projected onto the shell of the mill. If the grinding element impacts directly onto the lining, then accelerated wear of the lining and rapid degradation of the grinding media take place, without achieving any milling of the ore. It is therefore important that

the grinding elements are projected onto the toe of the charge; taking this into consideration, the impact point is emphasised in this work.

Because the theoretical model is based on the fundamental laws of motion, it can be applied to a mill of any size. All trajectories and angles of departure and impact are independent of the size, and can be directly scaled-up. However, it must be borne in mind that the pressures in the charge and the forces of impact increase with an increase in the size of the mill. So, for identical charge motions, different grinding characteristics apply for mills of different sizes.

So that more accurate predictions of the charge motion in a production mill can be given, measurements need to be made of the static and kinetic coefficients of friction for balls, rods, or rocks resting upon a lifter bar covered with slurry. In a pebble mill, the rocks rapidly round off to smooth oval shapes (as is easily observed by looking at the charge in such a mill), and can therefore be approximated by spheres. Therefore, the theoretical model can be directly applied in the prediction of the motion of the charge in a production mill.

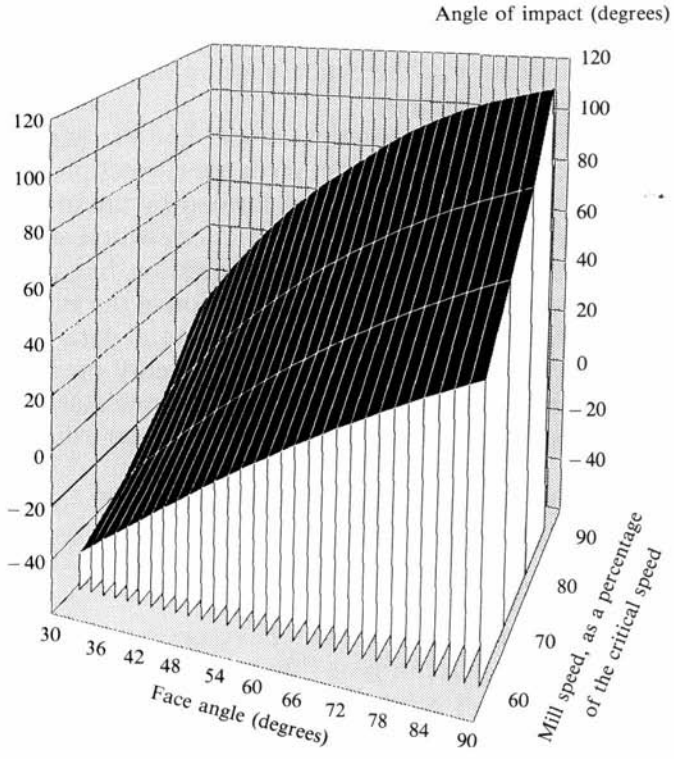

Fig. 18. The combined influence of the face angle of the lifter bar and the speed of the mill upon the angle of impact.

CONCLUSIONS

It was shown experimentally that when a smooth lining is used, extensive slip of the charge takes place. This results in the wasting of energy, accelerated liner wear, and inefficient charge motion. There is a tremendous increase in the height of the charge trajectories as the height of the lifter bars is increased from zero to slightly greater than the radius of a grinding element. To prevent the slipping of the charge on the liner, the lifter bar should be at least as high as the radius of a grinding element.

An increase in the height of the lifter bar beyond that of the radius of a grinding element, results in a slight increase in the height of the impact angle, which is then followed by a decrease. This effect has not been noted before, and is of considerable practical importance as it shows that a higher lifter bar is not going to project the charge to a point that is higher up the side of the mill. Therefore, the height of the lifter bars can be confidently increased in mills, without an increased risk of the balls impacting directly onto the shell of the mill.

An increase in the face angle of a lifter bar from a shallow angle up to an

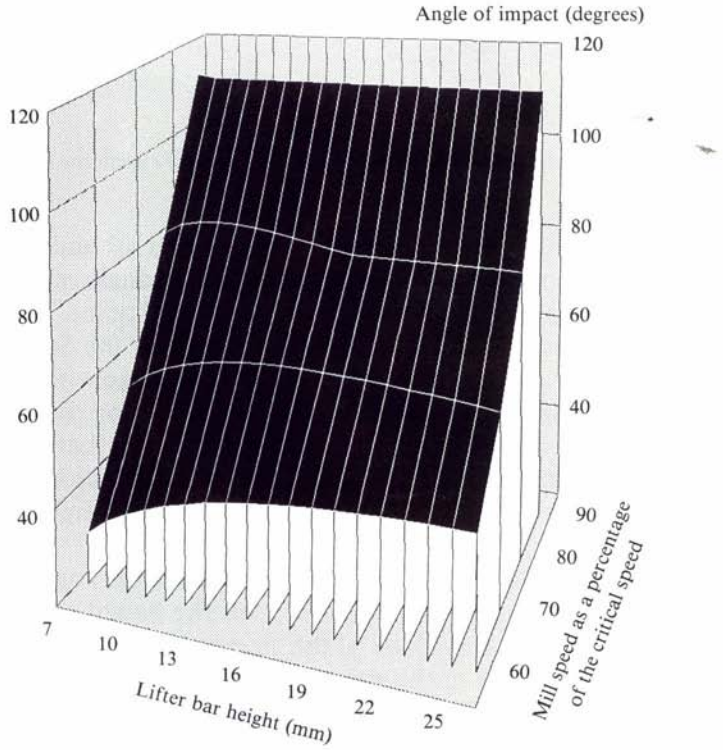

Fig. 19. The combined influence of the height of the lifter bar and the speed of the mill upon the angle of impact.

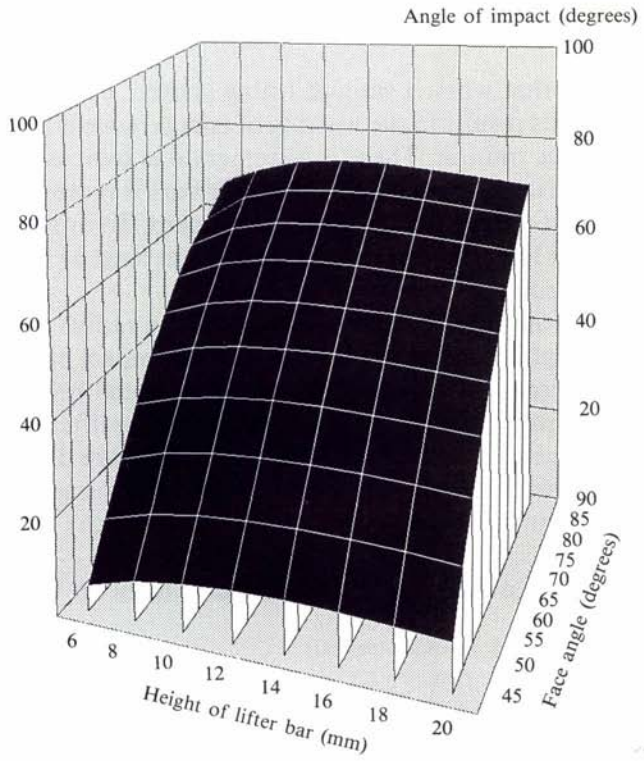

Fig. 20. The combined influence of the height of the lifter bar and the face angle upon the angle of impact.

angle of 90° (a rectangular profile), results in a greatly increased lift and impact angle of the grinding elements. By use of this effect, the face angle can be designed to allow the lifter bar to drop the charge onto any desired point. This is especially important in high-speed mills, such as are found on the South African gold mines, as lifter bars can be installed to key-in the charge without the projection of the charge onto the shell of the mill. A curved or round-tipped lifter bar yields an outer charge motion that is equivalent to that of a flat-faced lifter bar with a height that corresponds to the point at which the curvature starts. This height is equivalent to the minimum critical height, if the bar curves from its base.

There is a linear relationship between the speed of the mill and the angle of impact. The speed of the mill has a substantial effect on the height of the trajectories, and also on the motion of the bulk of the charge.

A comparison of the relative effects of the above-mentioned variables can be gained from the three-dimensional plots given in Figs. 18–20. The mill diameter is 387mm, and the range of each variable is given in accordance with the way in which that variable may be reasonably changed in a production mill.

ACKNOWLEDGEMENTS

This work is published by kind permission of Mintek. Discussions with, and comments by, Dr. L.A. Vermeulen are gratefully acknowledged as having enhanced this work.

REFERENCES

McIvor, R.E., 1983. Effects of speed and liner configuration on ball mill performance. Min. Eng., Jun: 617–622.

Powell, M.S., 1987. Survey of milling and mill lining practice on the South African gold mines. Mintek Rep. M350, Mintek, Randburg.

Powell, M.S., 1988. The effect of liner design upon charge motion in a rotary mill. MSc thesis, University of Cape Town, Cape Town.

Vermeulen, L.A., 1985. The lifting action of lifter bars in rotary mills. J.S. Afr. Inst. Min. Metall., 85 (2): 51–63.